Measurements beyond the diffraction limit: Far-field super-resolution imaging using scanning photonic nanojets

Karamehmedovic, Mirza

Publication date:
2023

Document Version
Publisher's PDF, also known as Version of record

Measurements beyond the diffraction limit: Far-field super-resolution imaging using scanning photonic nanojets

School of Physics on Optical Metrology

ICFO, 25 October 2023

Mirza Karamehmedović
Associate Professor

Department of Applied Mathematics and Computer Science
Technical University of Denmark
mika@dtu.dk

EURAMET

VILLUM FONDEN

Bibliography

- **Collaborators**
  - M. Karamehmedović and J. Glückstad. Phase-only steerable photonic nanojets. Opt. Express 31(17), 2023.
  - A. M. A. Alghamdi, P. Chen, and M. Karamehmedović. Optimal design of photonic nanojets under uncertainty. *To appear*, arXiv:2209.02454
  - M. Karamehmedović, K. Scheel, F. L.-S. Pedersen, A. Villegas, and P.-E. Hansen. Steerable photonic jet for super-resolution microscopy. Opt. Express 30(23), 2022.
  - N. M. B. Rehn, P.-E. Hansen, and M. Karamehmedović. Toward Photonic Nanojet Imaging for Microscopy. Proc. ACES 2023 Conference, Monterey, CA, USA.
  - M. Karamehmedović, K. Scheel, F. L.-S. Pedersen, and P.-E. Hansen. Imaging with a steerable photonic nanojet probe. Proc. SPIE 12203, Enhanced Spectroscopies and Nanoimaging 2022, 1220306 (3 October 2022); doi: 10.1117/12.2633442

- **Photonic jets (general)**
  - A. Darafsheh. Photonic nanojets and their applications. J. Phys. Photonics, 3:022001, 2021.
  - S. Lecler, S. Perrin, A. Leong-Hoi, and P. Montgomery. Photonic Jet Lens. Sci. Rep., 9:4725, 2019.
  - G. Huszka and M. A. M. Gijs. Super-resolution optical imaging: A comparison. MNE 2(7), 2019.

Bibliography

- **Enhanced backscattering**
  - A. Heifetz, K. Huang, A. V. Sahakian, X. Li, A. Taflove, and B. Vadim. Experimental confirmation of backscattering enhancement induced by a photonic jet. Appl. Phys. Lett., 89:221118, 2006.
  - Z. Chen and A. Taflove. Photonic nanojet enhancement of backscattering of light by nanoparticles: a potential novel visible-light ultramicroscopy technique. Opt. Express, 12(7):1214, 2004.
  - X. Li, Z. Chen, A. Taflove, and V. Backman. Optical analysis of nanoparticles via enhanced backscattering facilitated by 3-d photonic nanojets. Opt. Express, 13(2):526, 2005.

- **Fluorescence and Raman microscopy**
  - K. A. Sergeeva, M. V. Tutov, S. S. Voznesenskiy, N. I. Shamich, A. Yu. Mironenko, and A. A. Sergeeva. Highly-sensitive fluorescent detection of chemical compounds via photonic nanojet excitation. Sens. Actuators B Chem., 305:127354, 2020.
  - I. S. Ruzankina, and G. Ferrini. Enhancement of Raman signal by the use of BaTiO3 Microspheres. Proceedings - International Conference Laser Optics 2020. ICLO 2020:9285882, 2020.

- **Design of photonic jets**
  - J. Zhu and L. L. Goddard. Spatial control of photonic nanojets. Opt. Express 24(26): 30444, 2016.
  - A. Paganini, S. Sargheini, R. Hiptmair, and C. Hafner. Shape optimization of microlenses. Opt. Express 23(10):13099, 2015.
  - J. Huang, Y. Zhao, H. Yang, J. Wang, P. Briard, and Y. Han. Characteristics of photonic jets generated by a dielectric sphere illuminated by a Gaussian beam. Appl. Opt. 59(21):6390, 2020.

Plan

1. Definition of a photonic nanojet (PNJ)
2. PNJ steering by computed amplitude and phase of illumination
3. Phase-only PNJ steering
4. PNJs as scanning optical probes

Photonic nanojets (PNJs)

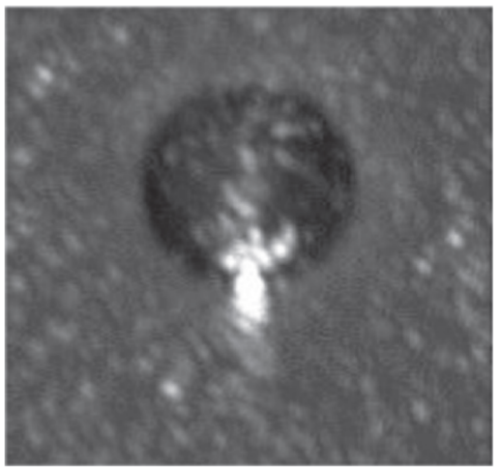

A photograph of an actual PNJ emerging behind an 8μm SiO_2 micro-disk illuminated at 532nm.
Liu, Physica E 73 (2015) 226—234, rotated.

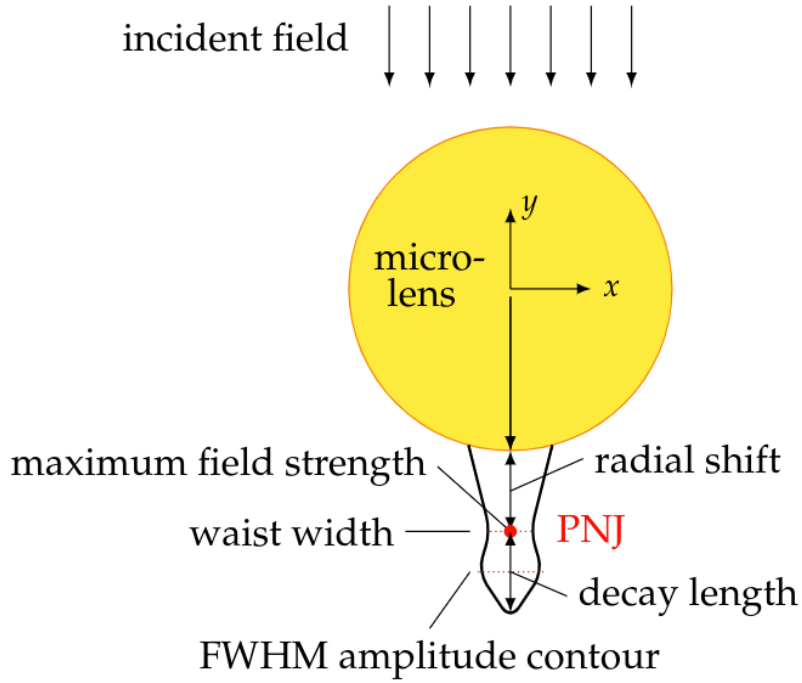

Definition of a PNJ and related quantities. The full width at half maximum (FWHM) amplitude contour is w.r.t. the amplitude of the total electric field.
Karamehmedović *et al.*, Opt. Express, 2022.

- allow highly localized measurement and excitation
- promising for label-free optical far-field super-resolution microscopy
- applicable also in fluorescence and Raman microscopy
- nanolithography; particle trapping; optical tweezers
- PNJ scanning with no opto-mechanical intervention?

PNJ steering by computed illumination of fixed micro-element

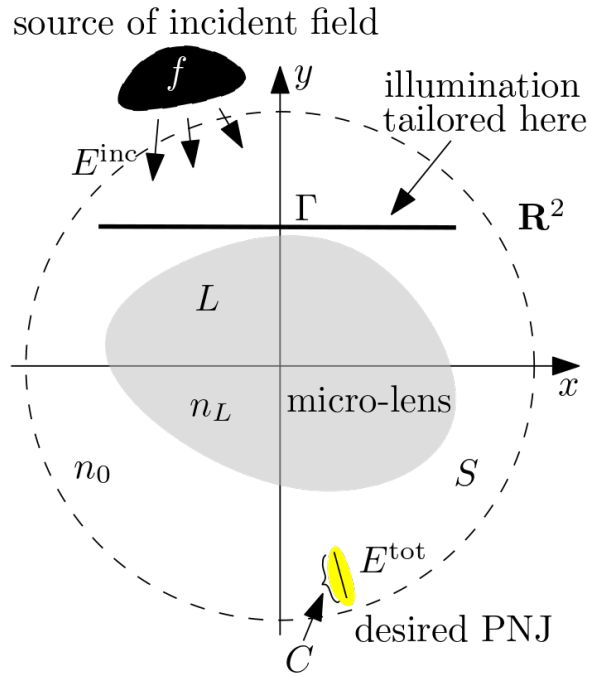

Karamehmedović *et al.*, Opt. Express, 2022.

- we consider the time-harmonic ($e^{j\omega t}$), 2D TE case
- λ_0: operating wavelength; $k_0 = 2\pi/\lambda_0$: wavenumber
- **inverse problem approach:** given E^{tot}, find E^{inc}
- define

$$\chi_L(\mathbf{x}) = \begin{cases} 1, & \mathbf{x} \in L, \\ 0 & \text{otherwise}, \end{cases} \qquad k(\mathbf{x}) = k_0[1 + \chi_L(\mathbf{x})(n_L - 1)], \quad \mathbf{x} \in \mathbf{R}^2.$$

- assume

$$\left.\begin{aligned} (\Delta + k(\mathbf{x})^2) E^{\text{tot}}(\mathbf{x}) &= f(\mathbf{x}), \quad \mathbf{x} \in \mathbf{R}^2, \\ E^{\text{tot}}(\mathbf{x}) &= \xi(\mathbf{x}), \quad \mathbf{x} \in C. \end{aligned}\right\} \tag{1}$$

with f supported outside S

PNJ steering by computed illumination of fixed micro-element

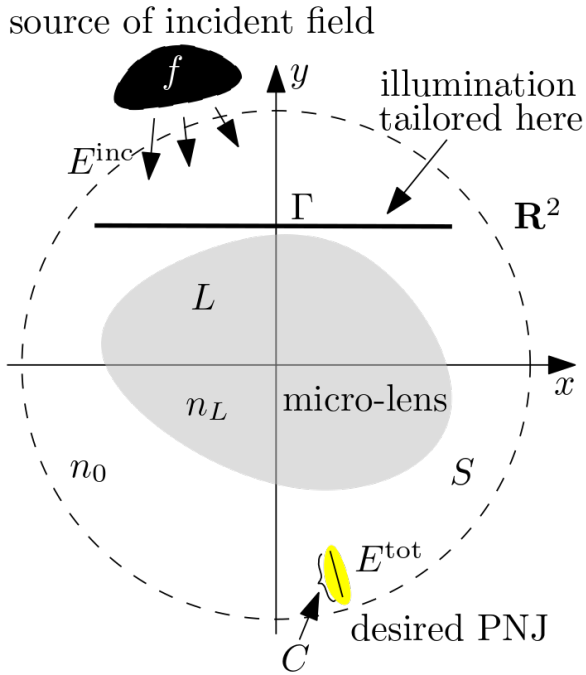

Karamehmedović *et al.*, Opt. Express, 2022.

- setting $E^{\text{tot}} = E^{\text{inc}} + E^{\text{sca}}$ with $(\Delta + k_0^2)E^{\text{inc}}(\mathbf{x}) = f(\mathbf{x})$ in $\mathbf{R}^2$, we get

$$\begin{aligned}(\Delta + k_0^2)E^{\text{tot}}(\mathbf{x}) &= f(\mathbf{x}) + (k_0^2 - k(\mathbf{x})^2)E^{\text{tot}}(\mathbf{x}) \\ &= (\Delta + k_0^2)E^{\text{inc}} - \alpha\chi_L(\mathbf{x})E^{\text{tot}}(\mathbf{x}),\ \mathbf{x} \in \mathbf{R}^2,\end{aligned}$$

  where $\alpha = k_0^2(n_L^2 - 1)$
- thus

$$(\Delta + k_0^2)E^{\text{sca}}(\mathbf{x}) = -\alpha\chi_L(\mathbf{x})E^{\text{tot}}(\mathbf{x}), \quad \mathbf{x} \in \mathbf{R}^2$$

PNJ steering by computed illumination of fixed micro-element

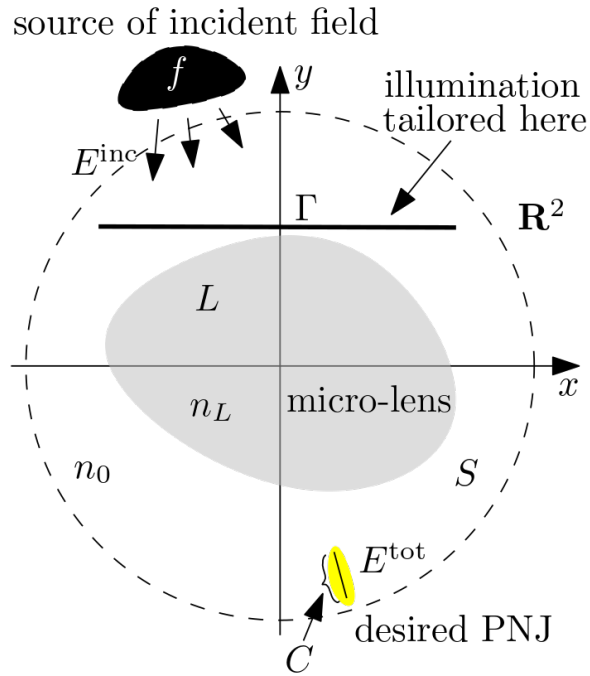

Karamehmedović *et al.*, Opt. Express, 2022.

- since E^{sca} must also satisfy the Sommerfeld radiation condition, this leads to

$$E^{\text{sca}}(\mathbf{x}) = -\alpha\Phi_0 * (\chi_L E^{\text{tot}})(\mathbf{x}) = -\alpha \int_{\mathbf{y}\in L} \Phi_0(\mathbf{x}-\mathbf{y}) E^{\text{tot}}(\mathbf{y}) d\mathbf{y}, \quad \mathbf{x} \in \mathbf{R}^2,$$

and hence to the Lippmann-Schwinger equation

$$E^{\text{inc}}(\mathbf{x}) = E^{\text{tot}}(\mathbf{x}) - E^{\text{sca}}(\mathbf{x}) = E^{\text{tot}}(\mathbf{x}) + \alpha \int_{\mathbf{y}\in L} \Phi_0(\mathbf{x}-\mathbf{y}) E^{\text{tot}}(\mathbf{y}) d\mathbf{y}, \quad \mathbf{x} \in \mathbf{R}^2. \quad (2)$$

Here $L^1_{\text{loc}}(\mathbf{R}^2) \ni \Phi_0(\mathbf{x}) = (j/4)H_0^{(2)}(k_0|\mathbf{x}|)$ is the unique radially outgoing fundamental solution of the Helmholtz operator $\Delta + k_0^2$ in $\mathbf{R}^2$, and $H_0^{(2)}$ is the Hankel function of the second kind and order zero.

PNJ steering by computed illumination of fixed micro-element

1. Define a neighborhood S of the micro-element L such that the desired PNJ is included in S. Pick a curve $C \subset S$ and a function ξ on C that represent the desired PNJ well via the second condition in (1). Also, pick a curve $\Gamma \subset S \setminus \overline{L}$ at which the tailored incident field is to be computed.
2. Solve the system in (1) (numerically) for the desired E^{tot} in S, recalling the assumption that $f \equiv 0$ in S. Prepare a program that approximates the numerical values of E^{tot} in L and at Γ.
3. Compute the incident field E^{inc} at Γ using (2) and the program from the previous step.
4. Illuminate the micro-element using a source f supported outside S, and that radiates a field approximating E^{inc} at Γ.

PNJ steering by computed illumination of fixed micro-element

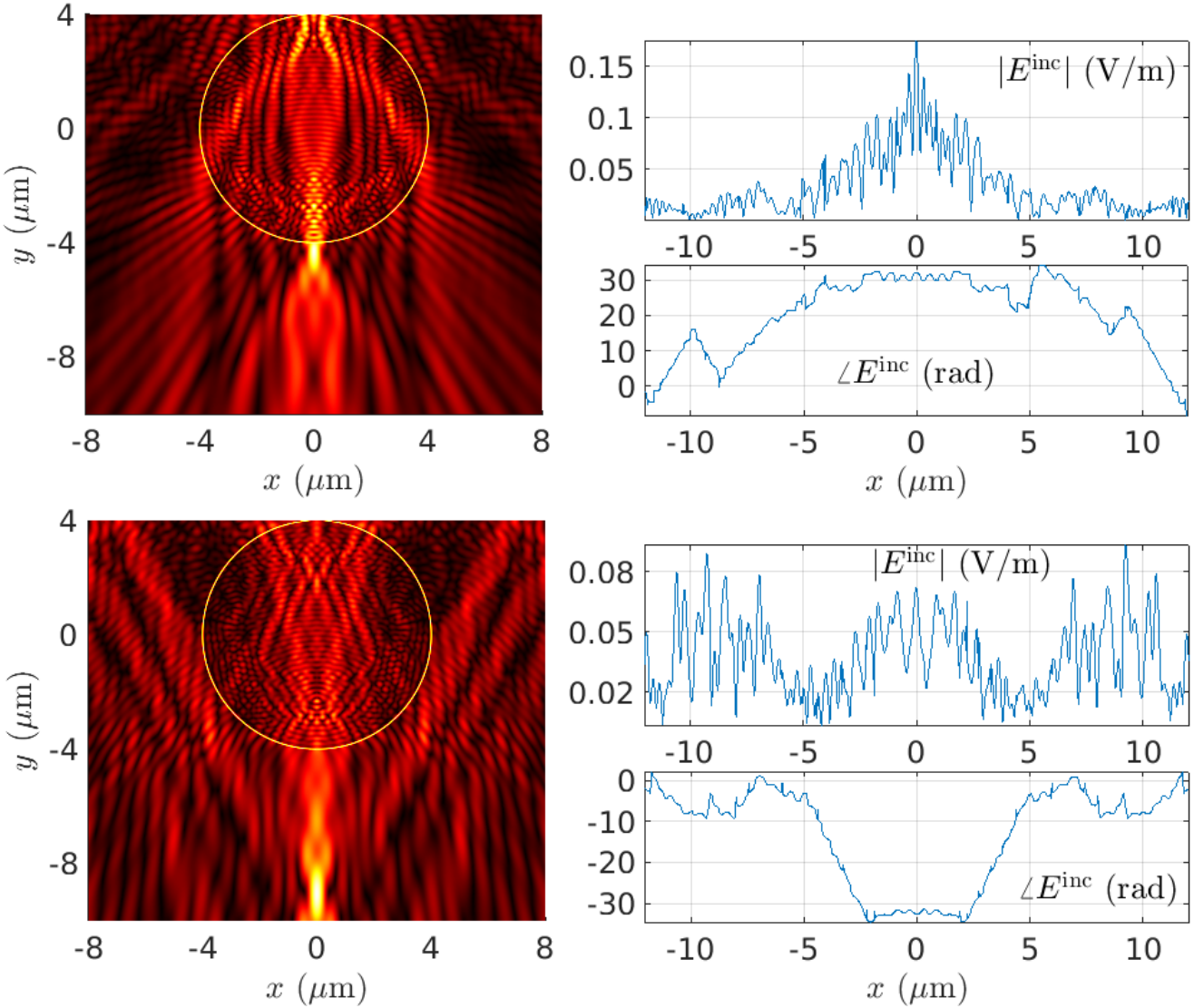

$\lambda_0 = 532$ nm, $n_L = 1.4607$ (SiO_2 micro-element), $R_{\text{lens}} = 4$ μm

Karamehmedović *et al.*, Opt. Express, 2022.

PNJ steering by computed illumination of fixed micro-element

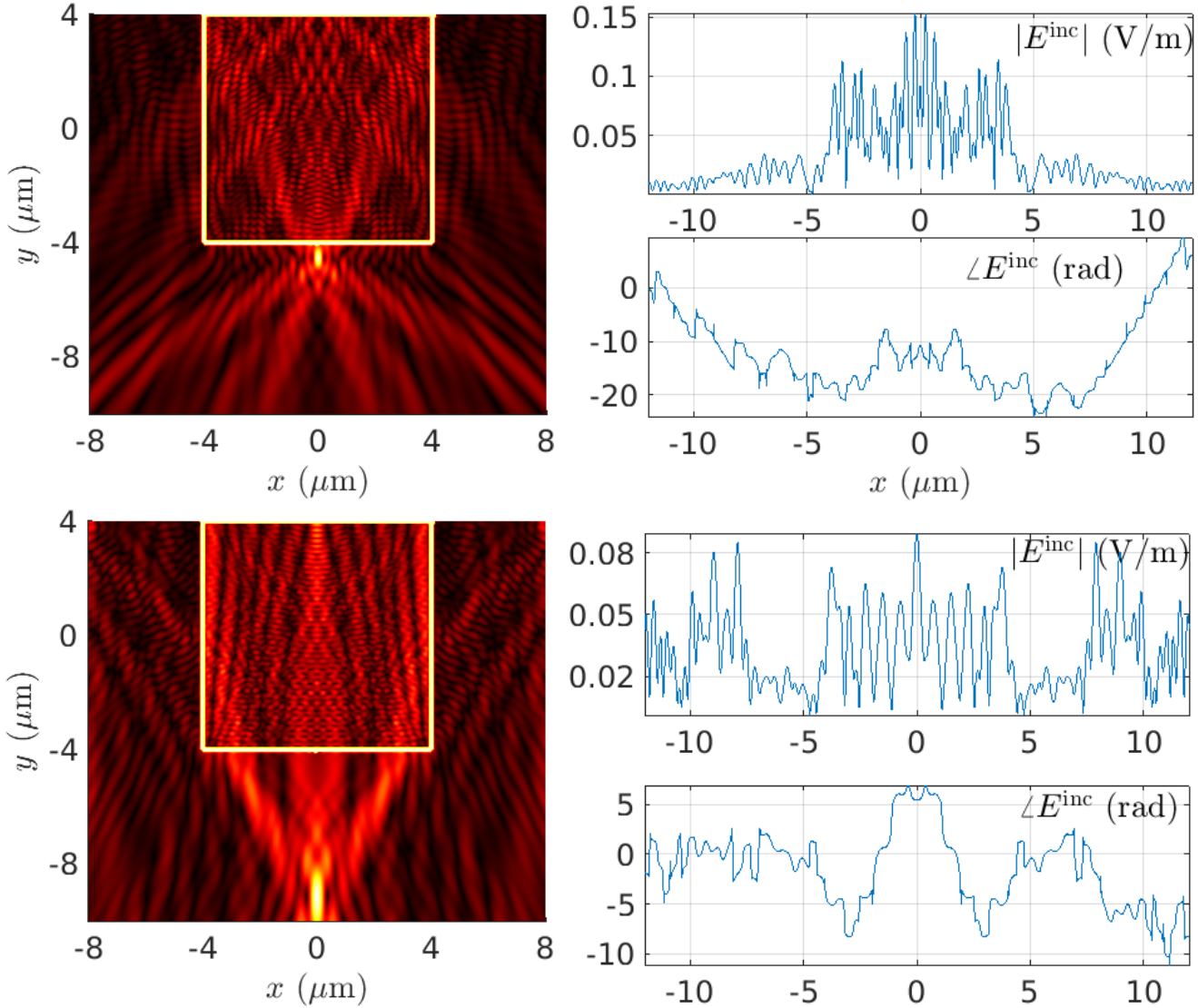

$\lambda_0 = 532$ nm, $n_L = 1.4607$ (SiO_2 micro-element), $a_{\text{lens}} = 8$ μm

Karamehmedović *et al.*, Opt. Express, 2022.

PNJ steering by computed illumination of fixed micro-element

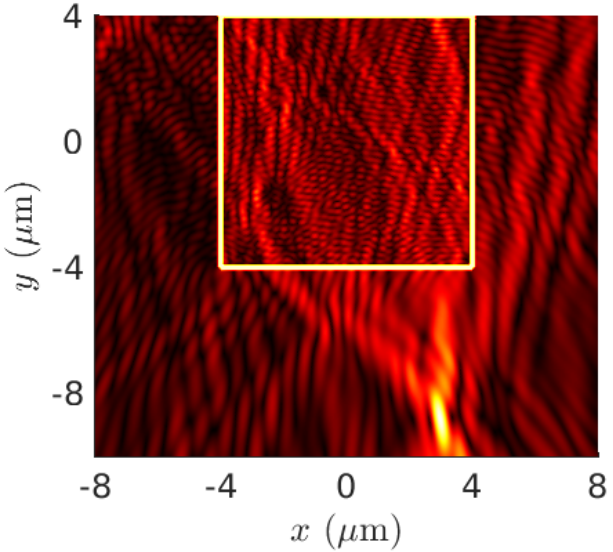

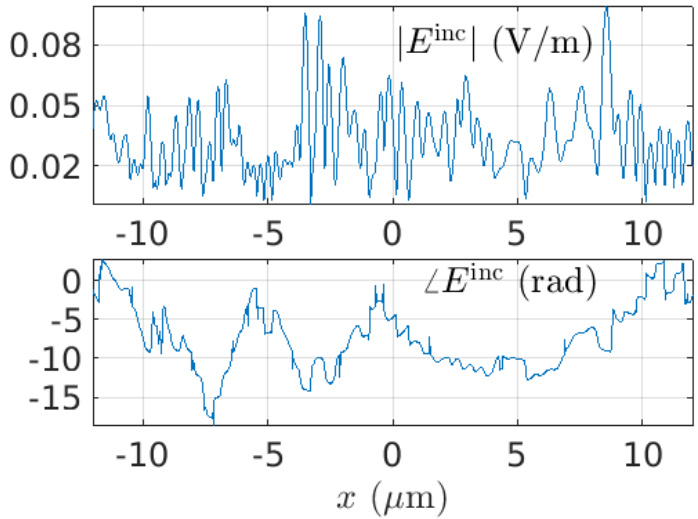

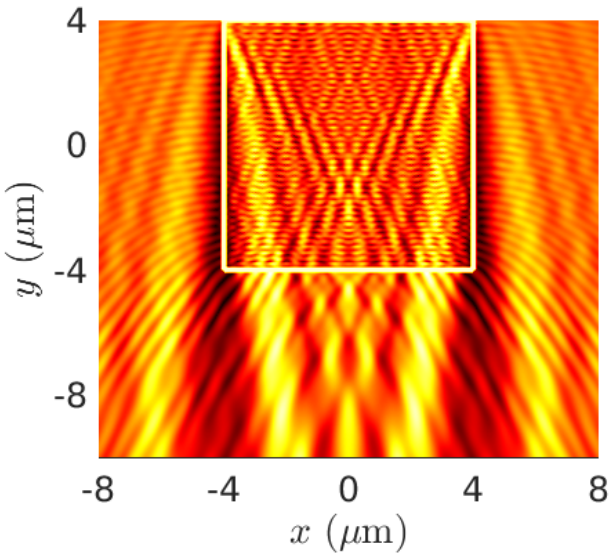

UPW illumination
along the negative y-axis

$\lambda_0 = 532$ nm, $n_L = 1.4607$ (SiO_2 micro-element), $a_{\text{lens}} = 8$ μm

Karamehmedović *et al.*, Opt. Express, 2022.

Achieving the amplitude and phase profiles of E^{inc} at Γ

- using phase filters or computer-generated holograms (CGHs) implemented with digital micromirror devices (DMDs) or liquid crystal spatial light modulators (SLMs)
- example:
  1. start with a Gaussian beam $u_0(\mathbf{x}) = A_0 \exp(-|\mathbf{x}|^2/w_0^2)$ with horizontal polarization along the horizontal direction
  2. a half-wave plate (HWP) rotates the polarization of the beam 45 deg so that it has equal components of magnitude $A_0/\sqrt{2}$ in the horizontal ($\hat{H}$) and vertical ($\hat{V}$) direction
  3. the first SLM imprints a phase $\varphi_1(\mathbf{x})$ to the horizontal component,

$$u(\mathbf{x}) = \frac{1}{\sqrt{2}} u_0(\mathbf{x})(e^{i\varphi_1(\mathbf{x})}\hat{H} + \hat{V}).$$

  4. a linear polarizer (LP) at 45 deg followed by a HWP modify the beam amplitude to $A_0(\exp(i\phi_1(\mathbf{x})) + 1)/2$ with the polarization state set to horizontal
  5. the second SLM imprints a phase $\varphi_2(\mathbf{x})$ such that, finally,

$$u(\mathbf{x}) = u_0(\mathbf{x}) \cos\left(\frac{\varphi_1(\mathbf{x})}{2}\right) \exp i\left(\frac{\varphi_1(\mathbf{x}) + 2\varphi_2(\mathbf{x})}{2}\right)$$

- 8-bit SLMs can in principle produce phase distributions φ_1, φ_2 discretized in steps of 2π rad/255$\approx$24.6 mrad ($\approx$1.4 deg)

PNJ steering by computed illumination of fixed micro-element

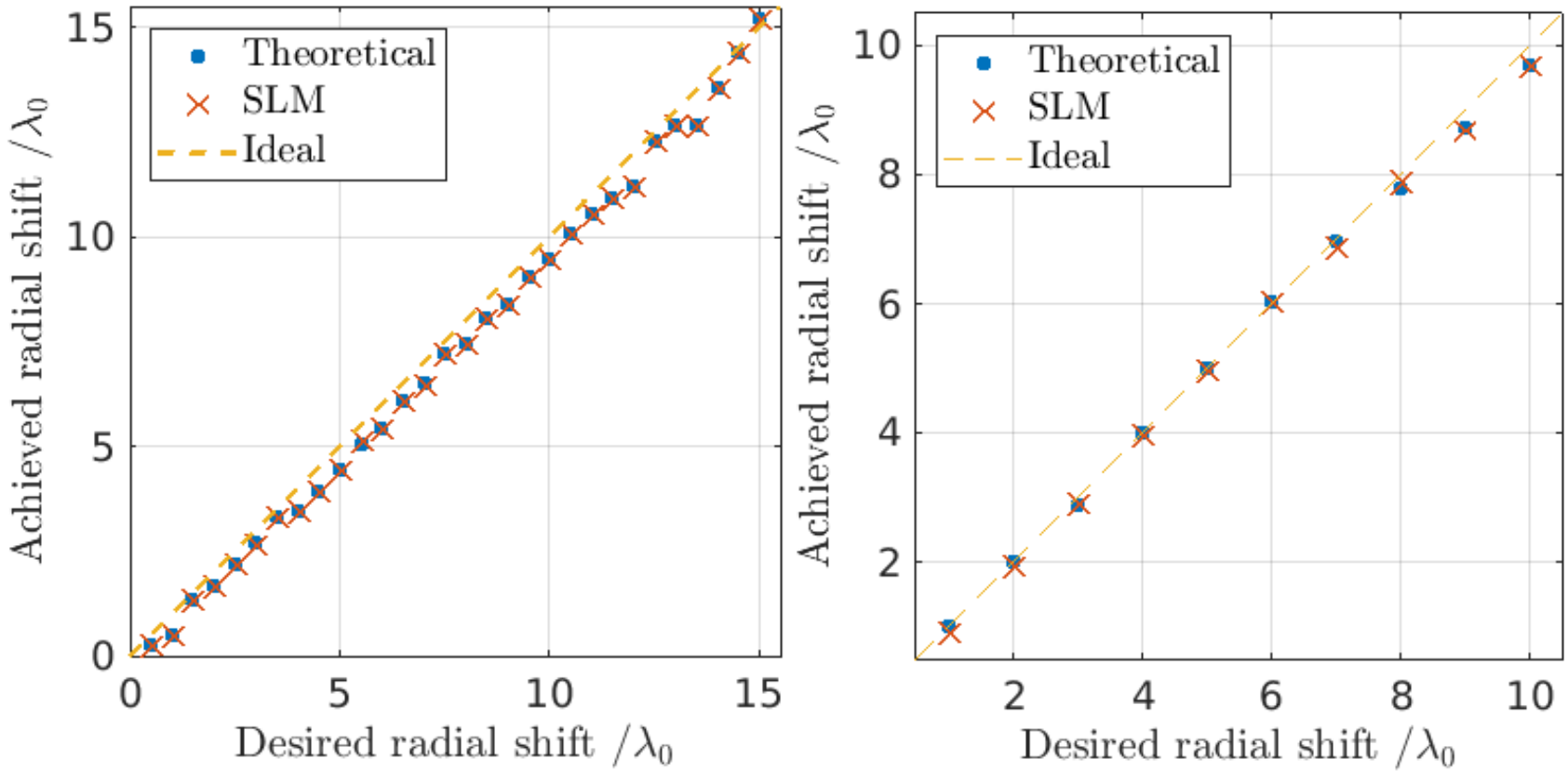

Left: circular micro-element, right: square micro-element.

Mean relative error for circular micro-element: 9.9% for theoretical and SLM incident fields.

Mean relative error for square micro-element: 1.5% for theoretical and 2.7% for SLM incident fields.

Karamehmedović *et al.*, Opt. Express, 2022.

PNJ steering by computed illumination of fixed micro-element

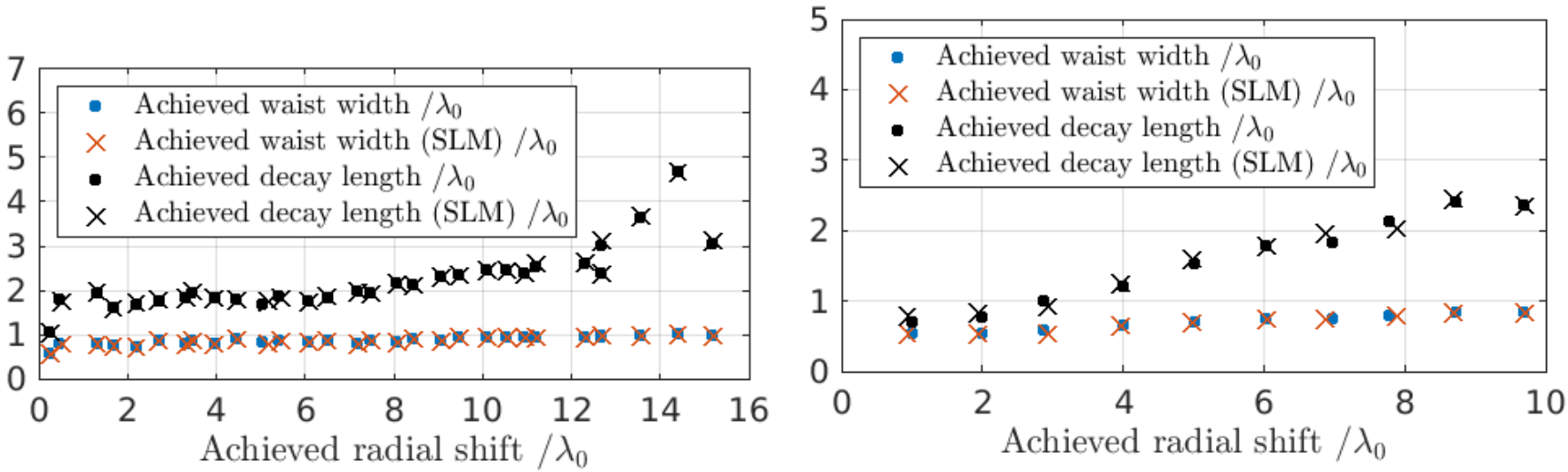

Left: circular micro-element, right: square micro-element.

	circular micro-lens	circular micro-lens (SLM)	square micro-lens	square micro-lens (SLM)
mean waist width	$0.88\lambda_0$	$0.88\lambda_0$	$0.70\lambda_0$	$0.70\lambda_0$
mean decay length	$2.22\lambda_0$	$2.24\lambda_0$	$1.58\lambda_0$	$1.60\lambda_0$

Karamehmedović *et al.*, Opt. Express, 2022.

Phase-only PNJ steering

Karamehmedović and Glückstad, Opt. Express, 2023.

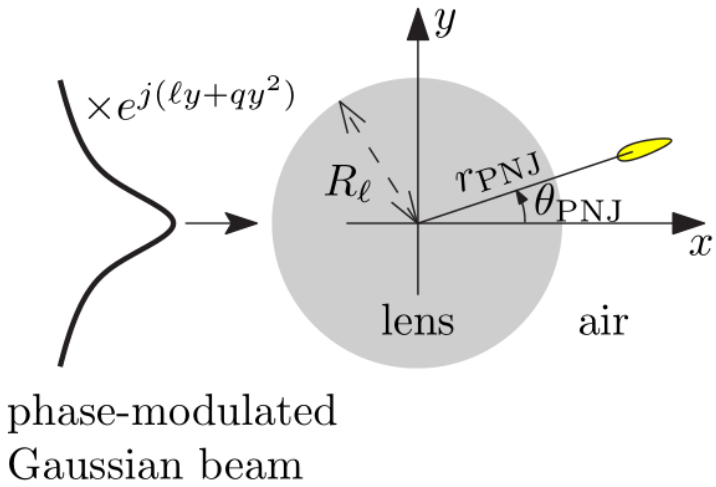

Fixed Gaussian laser beam (paraxial approximation):

$$E^{\text{laser}}(x,y) = \sqrt{\frac{w_0}{w(x)}}\, e^{-y^2/w(x)^2 - jk(x,y)x - jk(x,y)y^2/2R(x) + j\eta(x)/2}.$$

Here $k(x,y)$ is the wavenumber satisfying

$$k(x,y) = \begin{cases} 2\pi/\lambda_0 & \text{outside micro-element,} \\ (2\pi/\lambda_0)n_\ell & \text{inside micro-element;} \end{cases}$$

$w(x)$ is the beam radius given by

$$w(x) = w_0\sqrt{1+\left(\frac{x-p_0}{x_0}\right)^2}; \tag{3}$$

Phase-only PNJ steering

Karamehmedović and Glückstad, Opt. Express, 2023.

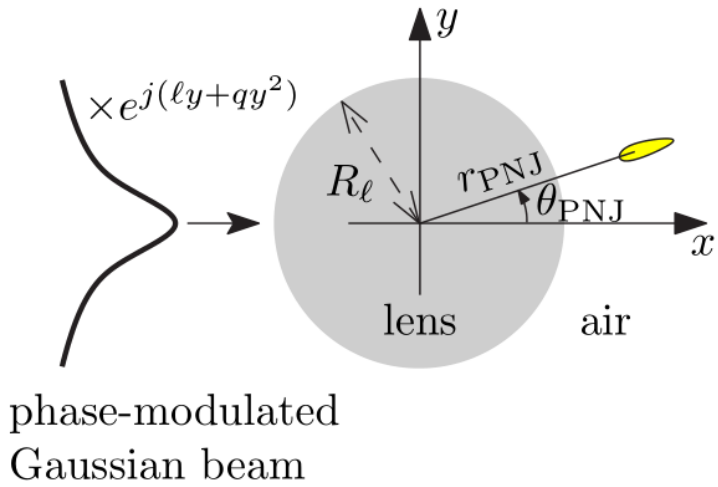

Fixed Gaussian laser beam (paraxial approximation):

$$E^{\text{laser}}(x,y) = \sqrt{\frac{w_0}{w(x)}}\, e^{-y^2/w(x)^2 - jk(x,y)x - jk(x,y)y^2/2R(x) + j\eta(x)/2}.$$

$p_0 = -R_\ell = -2.5$ μm is the beam focus along the x-axis; $w_0 = 2\lambda_0 = 1.064$ μm is the beam waist radius (the beam radius at focus $x = p_0$); $R(x)$ is the beam wavefront curvature radius given by

$$R(x) = (x - p_0)\left(1 + \left(\frac{x_0}{x - p_0}\right)^2\right); \tag{4}$$

$\eta(x)$ is the Gouy phase given by

$$\eta(x) = \arctan\left(\frac{x - p_0}{x_0}\right); \tag{5}$$

Phase-only PNJ steering

Karamehmedović and Glückstad, Opt. Express, 2023.

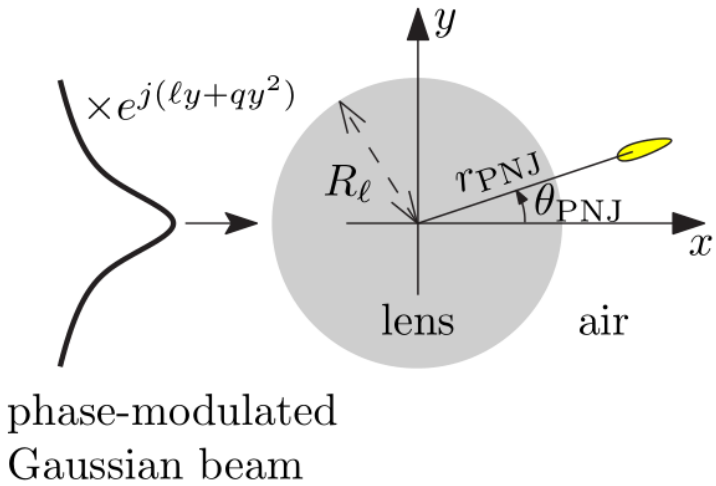

Fixed Gaussian laser beam (paraxial approximation):

$$E^{\text{laser}}(x,y) = \sqrt{\frac{w_0}{w(x)}}\, e^{-y^2/w(x)^2 - jk(x,y)x - jk(x,y)y^2/2R(x) + j\eta(x)/2}.$$

... and finally

$$x_0 = \frac{k(x,y)w_0^2}{2}. \tag{6}$$

Phase-only PNJ steering

Karamehmedović and Glückstad, Opt. Express, 2023.

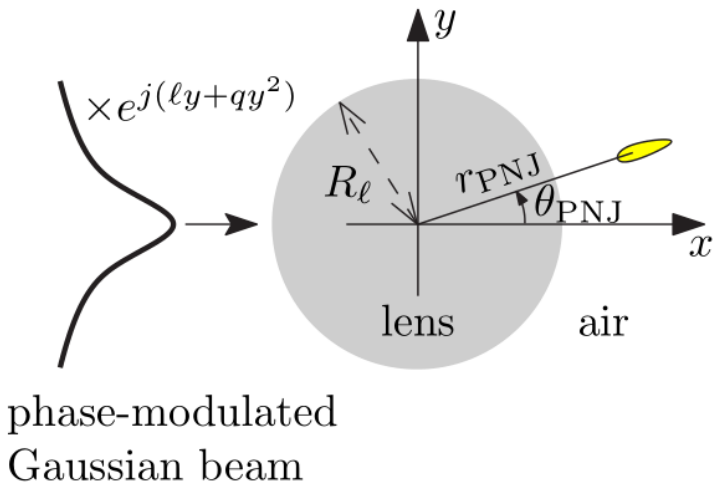

Phase-modulated incident field:

$$E^{\mathrm{inc}}(x,y) = e^{j\varphi(y)} E^{\mathrm{laser}}(x,y)$$

Transversal phase shift:

$$\varphi(y) = \ell y + q y^2$$

The parameters ℓ and q impose a transverse linear and quadratic phase modulation, respectively, of the incident Gaussian beam.

Phase-only PNJ steering

Karamehmedović and Glückstad, Opt. Express, 2023.

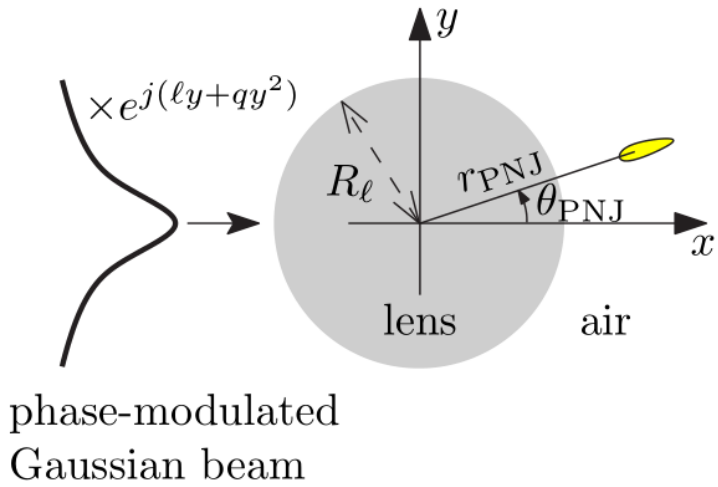

- a simple empirical PNJ steering algorithm
- interpolate a pre-computed table $(\ell, q) \leftrightarrow (r_{\mathrm{PNJ}}, \theta_{\mathrm{PNJ}})$:
  1. compute the total near fields for (ℓ, q) over some chosen grid;
  2. for each (ℓ, q) find the resulting PNJ coordinates $(r_{\mathrm{PNJ}}, \theta_{\mathrm{PNJ}})$
  3. find a fit vector function $F(r_{\mathrm{PNJ}}, \theta_{\mathrm{PNJ}})$ for the mapping $(r_{\mathrm{PNJ}}, \theta_{\mathrm{PNJ}}) \mapsto (\ell, q)$ over an appropriate dynamical range
  4. given desired PNJ coordinates $(r_{\mathrm{PNJ}}, \theta_{\mathrm{PNJ}})$, estimate the corresponding $(\ell, q) \approx F(r_{\mathrm{PNJ}}, \theta_{\mathrm{PNJ}})$ and apply the transverse phase modulation $\exp j(\ell y + qy^2)$ to the incident Gaussian beam

Phase-only PNJ steering

Karamehmedović and Glückstad, Opt. Express, 2023.

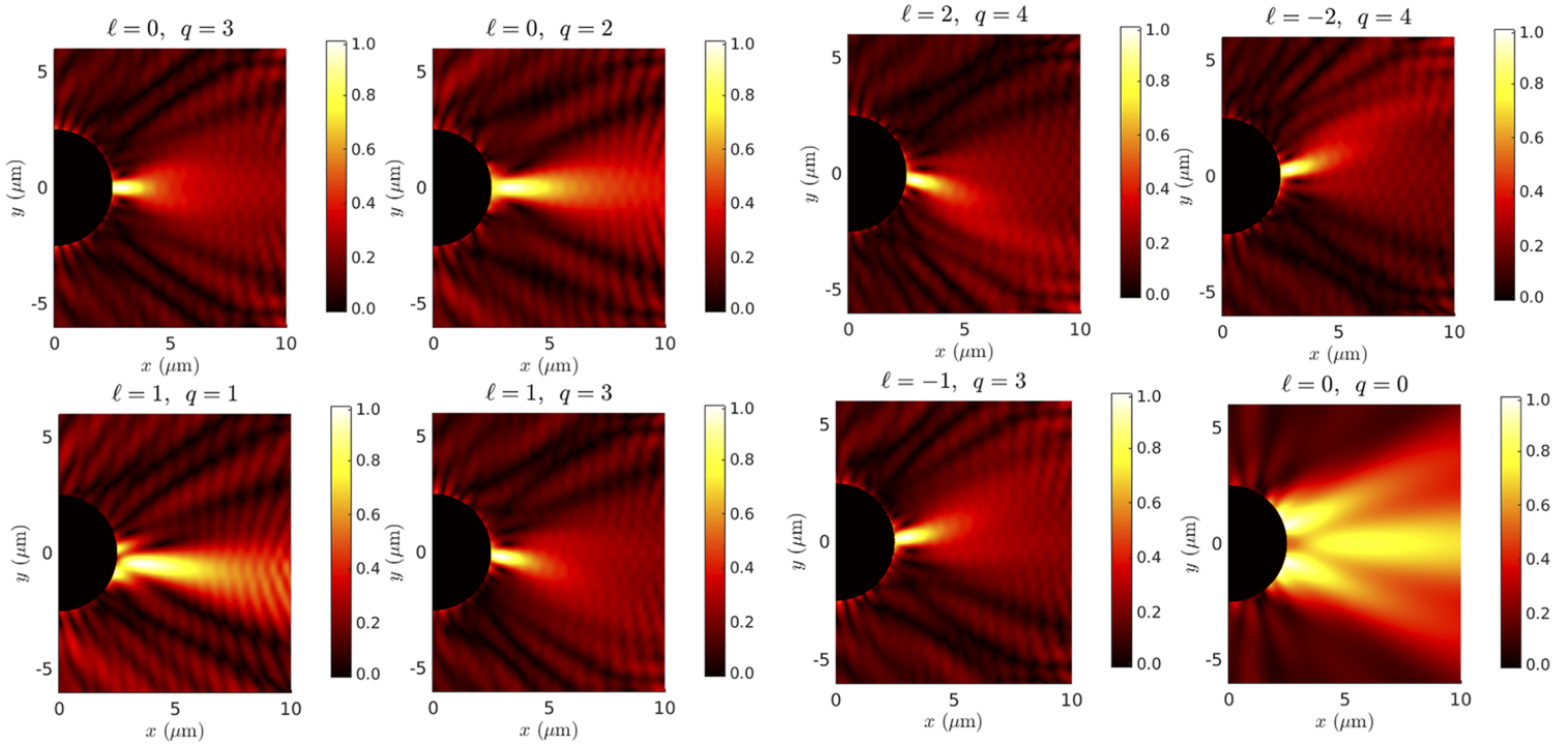

Fig. 2. PNJ steering by phase-only modulation of a fixed incident Gaussian beam, with $[\ell] = \mu\mathrm{m}^{-1}$ and $[q] = \mu\mathrm{m}^{-2}$. The total electric fields shown are normalized to maximum amplitude of 1 V/m. The bottom right image ($\ell = 0\ \mu\mathrm{m}^{-1}$, $q = 0\ \mu\mathrm{m}^{-2}$) results from illumination by the unmodulated Gaussian beam, and is not confined to a single high-intensity area.

$$\lambda_0 = 532\ \mathrm{nm},\ n_\ell = 1.49,\ R_\ell = 2.5\ \mu\mathrm{m}$$

- lossless
- uses only one SLM/phase mask

Phase-only PNJ steering

Karamehmedović and Glückstad, Opt. Express, 2023.

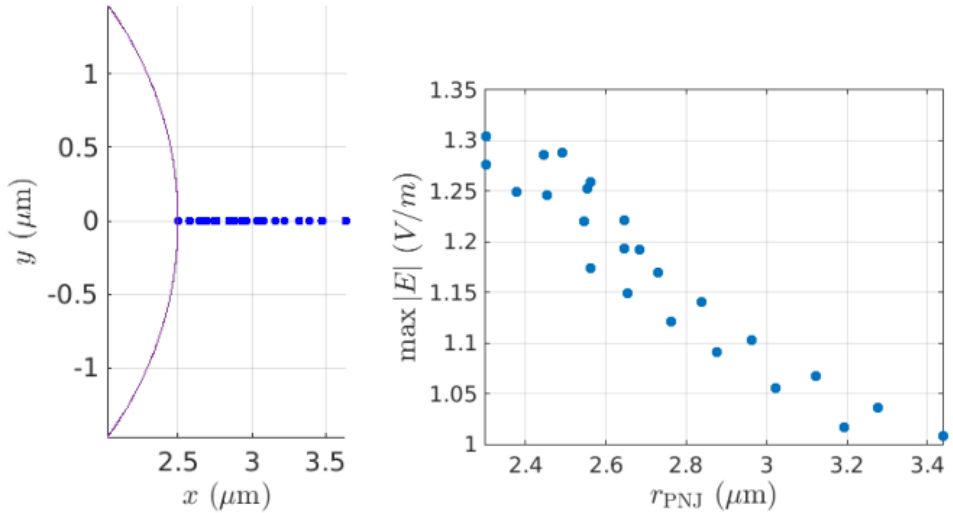

Fig. 4. Left: PNJ positions with phase modulation factors (ℓ, q) for $\ell = 0\ \mu\mathrm{m}^{-1}$, $q = 1.7, 1.8, \ldots, 4\ \mu\mathrm{m}^{-2}$. Right: The PNJ peak electric field amplitudes.

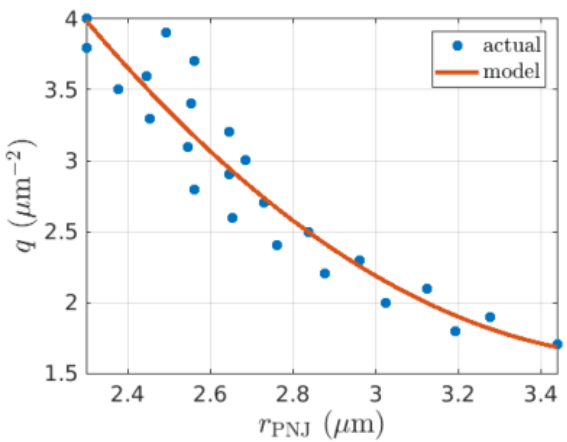

Fig. 5. Fitting the function $q(r_{\mathrm{PNJ}})$ for $\ell = 0$, see Eq. (9).

$$q(r_{\mathrm{PNJ}}) \approx 1.251 \cdot r_{\mathrm{PNJ}}^2 - 9.704 \cdot r_{\mathrm{PNJ}} + 20.43$$

Phase-only PNJ steering

Karamehmedović and Glückstad, Opt. Express, 2023.

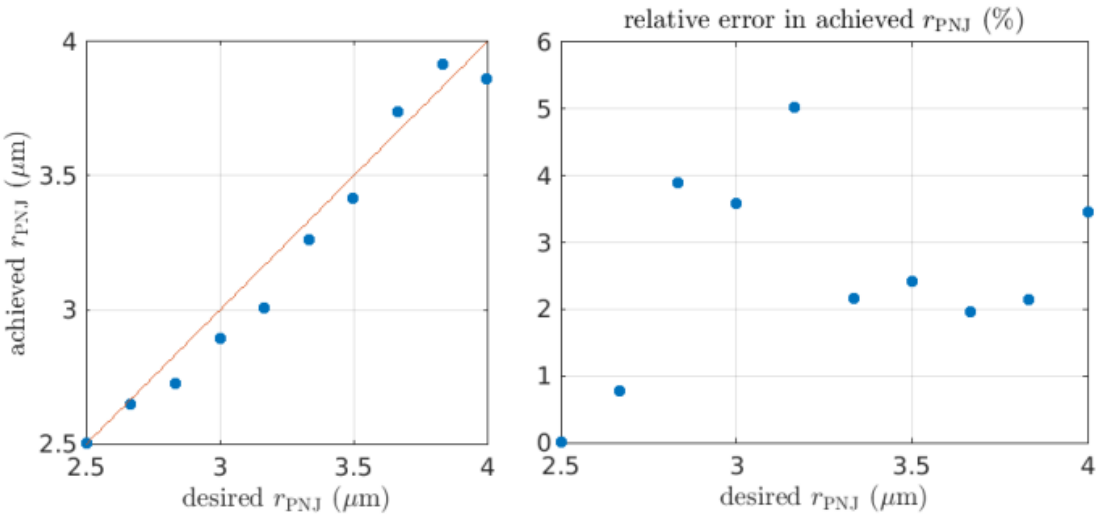

Fig. 6. Radial (axial) control of PNJ position. Left: desired vs. achieved PNJ radial coordinates r_{PNJ}. The straight linear piece is the ideal. Right: the relative error in the achieved r_{PNJ}. The mean relative error here is 2.54% and the maximum relative error is 5.02%.

Phase-only PNJ steering

Karamehmedović and Glückstad, Opt. Express, 2023.

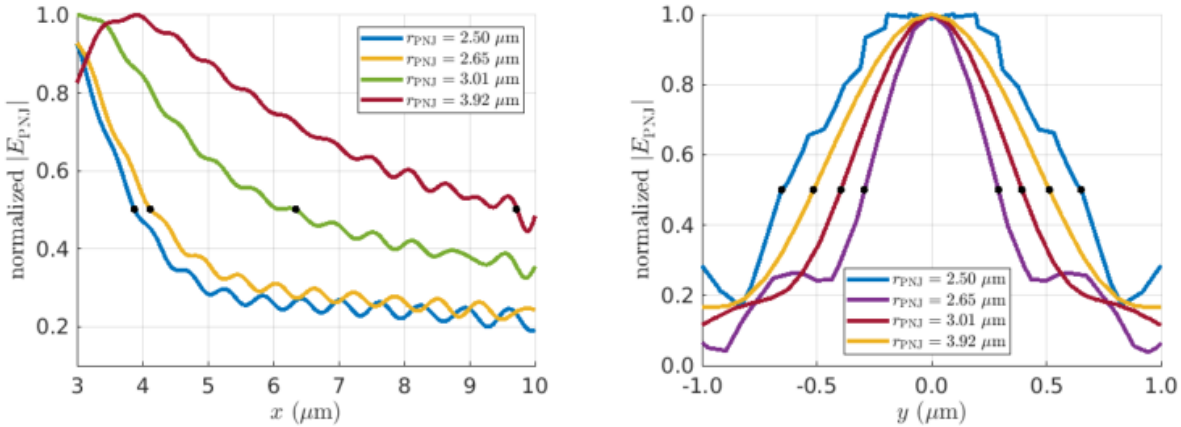

Fig. 7. Longitudinal profiles (left) and transverse profiles (right) of some of the achieved PNJs. Decay length is measured from the location of the field maximum to the location of the first half-maximum (black dot). The waist width is the distance between the two half-maxima (black dots).

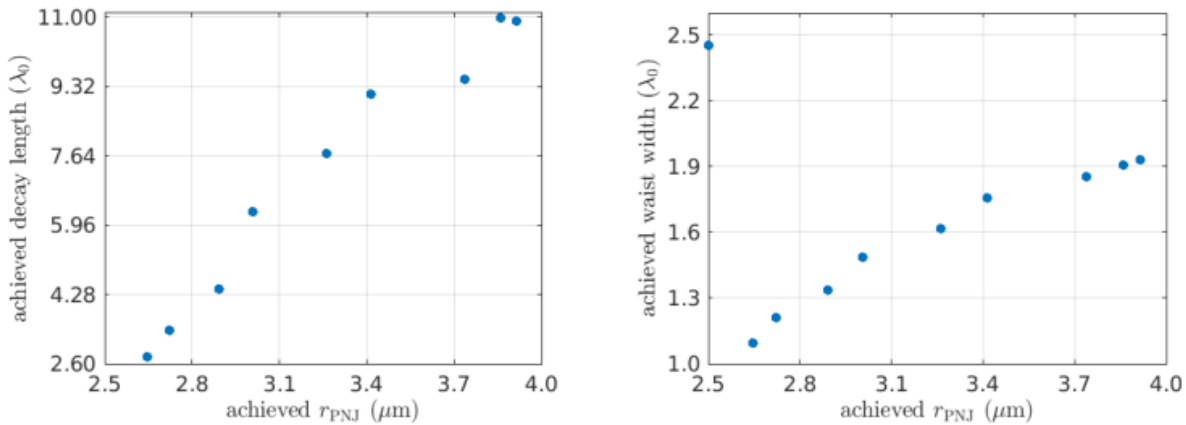

Fig. 8. Decay lengths and waist widths of the achieved PNJs, relative to the operating wavelength $\lambda_0 = 532$ nm.

PNJ as a scanning optical probe

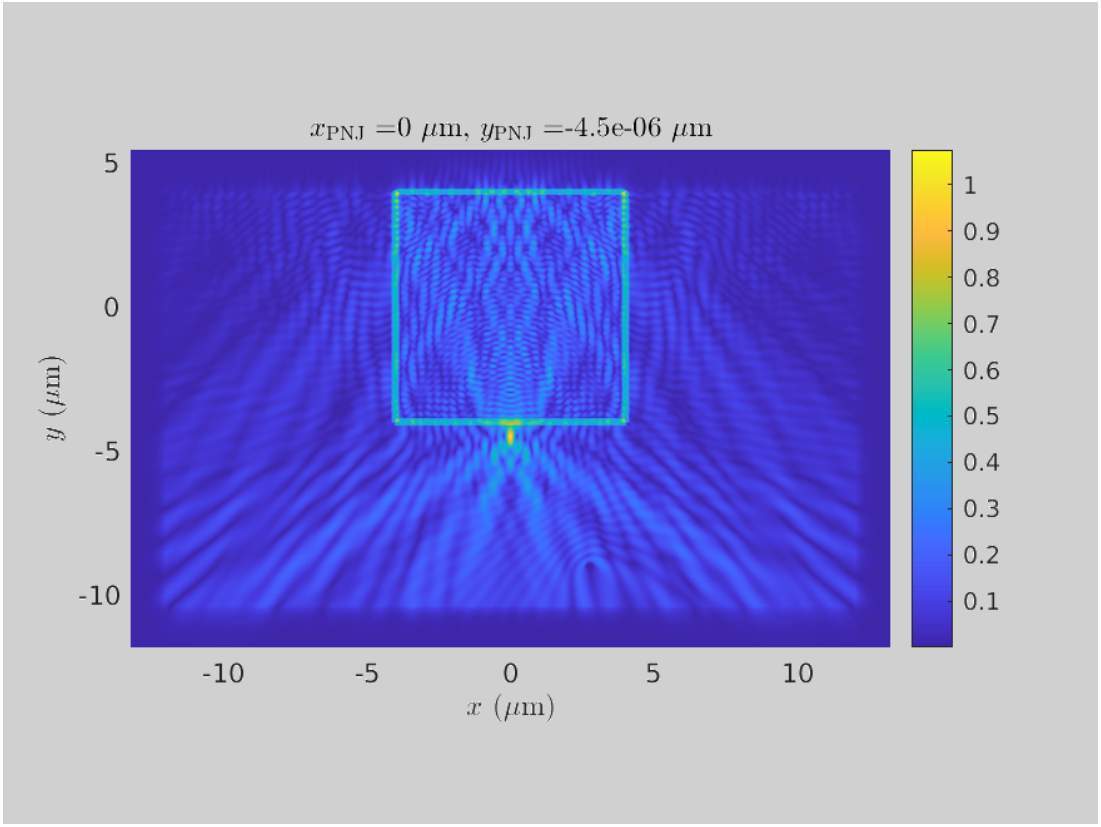

Vertical super-resolution: thin films

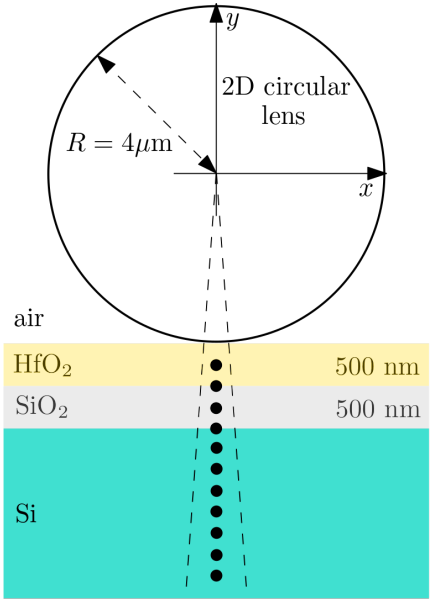

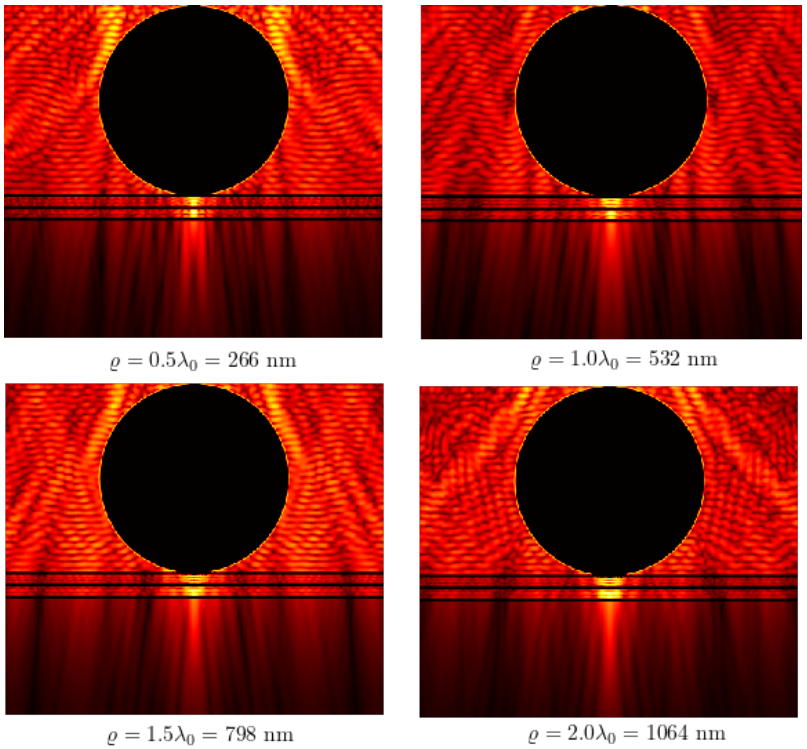

Left: Probing a two-layered thin film on a substrate with a steerable PNJ produced by a 2D circular cross-section homogeneous dielectric (SiO_2) micro-element. The far field amplitude is sampled at ± 3.8 deg from the negative y-axis, as sketched. The thick black points in the figure sketch the PNJ probe positions (separation $\lambda_0/2 = 266$ nm). Right: Computed near-field images at the indicated PNJ radial shifts ϱ. The thick black lines show the material interfaces.

$\lambda_0 = 532$ nm, $n_{HfO_2} = 1.9044$, $n_{SiO_2} = 1.4607$, $n_{Si} = 4.1520$, $k_{Si} = 0.051787$

Karamehmedović *et al.*, Proc. SPIE, 2022.

Vertical super-resolution: thin films

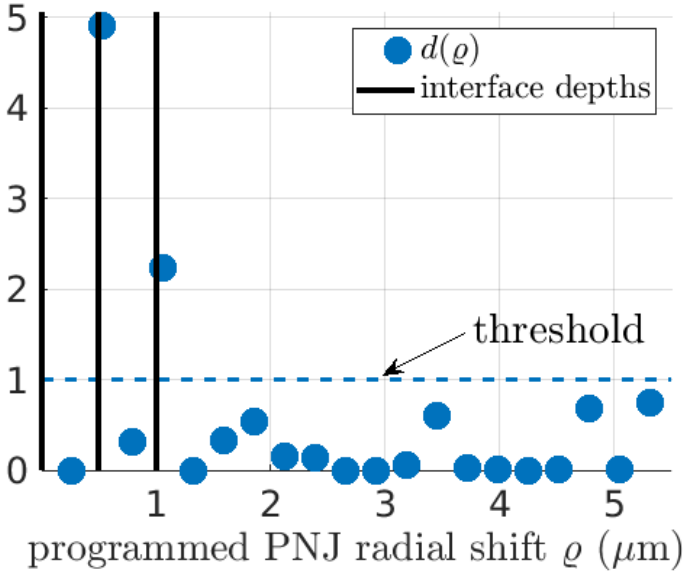

- $d(\varrho) = \left(|E^{\text{far}}_{\text{direct};\varrho}|/1.1|E^{\text{far}}_{\text{second};\varrho}|\right)^4$ if the second peak in $|E^{\text{far}}_{\varrho}|$ is within ± 1.5 deg from negative y-axis
- $d(\varrho) = 0$ otherwise
- 6.4% relative error using 266 nm steps in PNJ scanning

- this function attains values greater than 1 precisely when the measured direct-transmission far field is stronger than all far-field side lobes within ± 3.8 deg from direct transmission, and when furthermore the most dominant side lobe is within ± 1.5 deg from direct transmission
- the magnitude and direction of the far field are linked to the Fresnel reflections and the shape of the wavefront at the interface. A nearly planar wavefront at the interface results in a high direct transmission far-field value. Thus, we choose to interpret the case with dominant direct-transmission and near-direct-transmission far field as the PNJ hitting a material interface.
- vertical resolution limit in air: $2\lambda_0/\text{NA}^2 \approx 1180$ nm for NA$= 0.95$ and $\lambda_0 = 532$ nm (Novotny and Hecht, *Principles of Nano-Optics*, 2019.)

Karamehmedović *et al.*, Proc. SPIE, 2022.

Lateral super-resolution: isolated particles

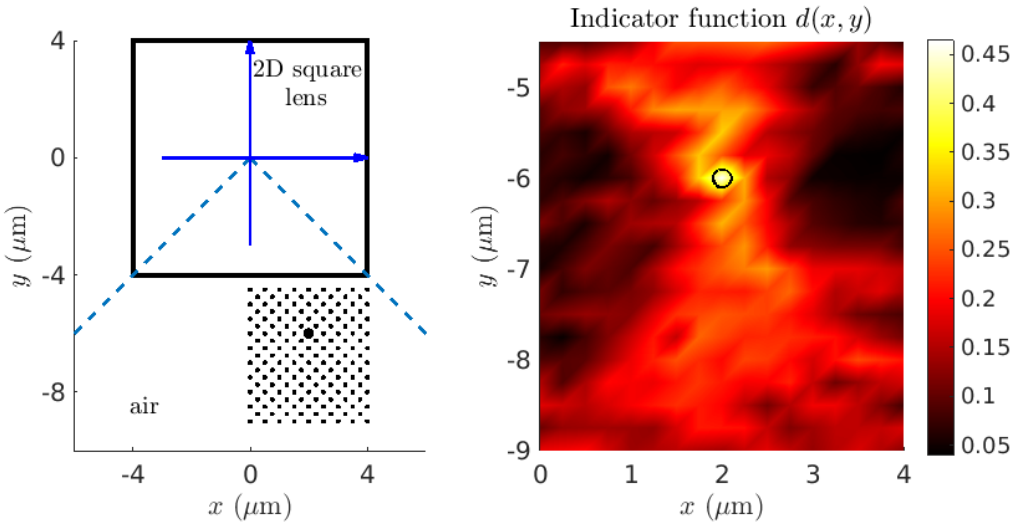

Left: Scanning an area containing a nanoparticle using a PNJ probe produced by a 2D homogeneous dielectric (SiO_2) micro-element with a square 8 μm cross-section. The nanoparticle is marked with the thick point. The grid of thin points shows the PNJ probing positions (x- and y-separation 250 nm). The far field amplitude is sampled at ± 45 deg from the negative y-axis, as displayed. Right: The resulting localization of the nanoparticle (outlined in black).

$\lambda_0 = 532$ nm, $n_{\text{Au}} = 0.54386$, $k_{\text{Au}} = 2.2309$

$R_{\text{part}} = 100$ nm, $x_{\text{part}} = 2$ μm, $y_{\text{part}} = -6$ μm

$E^{\text{far}}_{\text{part};(x,y)}$: the far field of particle illuminated by sample-free PNJ field at (x, y)

$E^{\text{far}}_{0;(x,y)}$: the far field of sample-free PNJ field at (x, y)

$$d(x,y) = \frac{\| \, |E^{\text{far}}_{\text{part};(x,y)}| - |E^{\text{far}}_{0;(x,y)}| \, \|_2}{\| \, |E^{\text{far}}_{0;(x,y)}| \, \|_2}.$$

Karamehmedović *et al.*, Proc. SPIE, 2022.

Lateral super-resolution: isolated particles

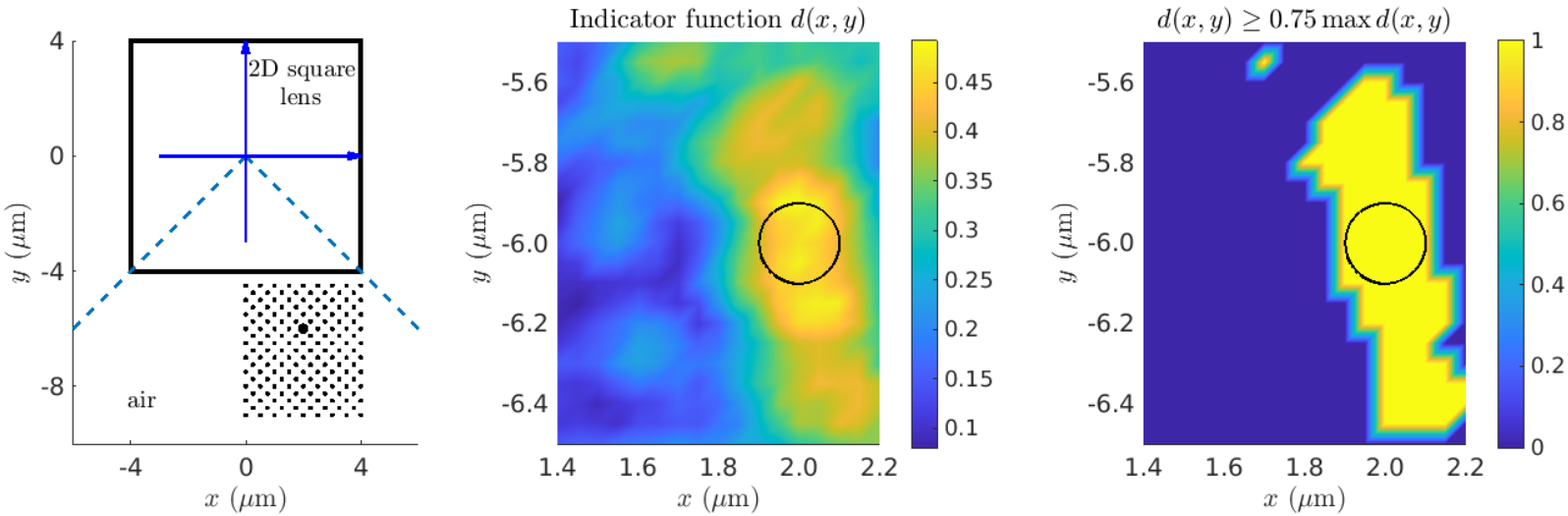

A zoomed-in image of the gold nanoparticle (outlined in black) computed using a finer (50 nm) PNJ probe grid. Distance of NP center from micro-element: 2 μm.

Approximate PNJ probe dimensions: waist width $0.70\lambda_0 \approx 372$ nm, decay length $1.58\lambda_0 \approx 841$ nm.

Lateral resolution (Abbe) limit in air: $\lambda_0/2\text{NA} = 280$ nm for NA$= 0.95$ and $\lambda_0 = 532$ nm. (Born and Wolf, *Principles of Optics*, 1997.)

Karamehmedović *et al.*, Proc. SPIE, 2022.

Lateral super-resolution: isolated particles

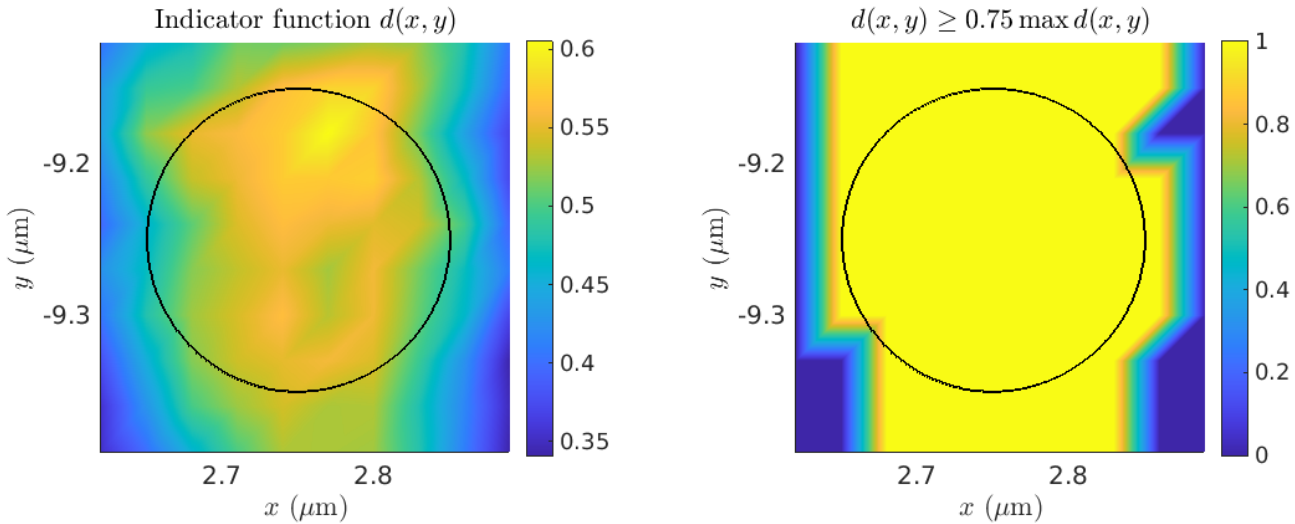

A zoomed-in image of the gold nanoparticle (outlined in black) computed using a 30 nm PNJ probe grid and a square SiO_2 micro-element with side length 16 μm. Distance of NP center from micro-element: 1.25 μm.

Lateral resolution (Abbe) limit in air: $\lambda_0/2\text{NA} = 280$ nm for $\text{NA} = 0.95$ and $\lambda_0 = 532$ nm. (Born and Wolf, *Principles of Optics*, 1997.)

Resolving sub-classical lateral gaps

Karamehmedović and Hansen, Bremen Zoom Workshop 2023.

- 2D TE; $\lambda_0 = 532$ nm;
- square SiO_2 micro-element; $a_{\text{lens}} = 15$ μm;
- two circular gold (Au) nanoparticles; $R_{NP} = 100$ nm; $d_{\text{gap}} = 200$ nm; $d_{\text{Abbe}} = 280$ nm;
- $(x_{\text{NP}}, y_{\text{NP}}) = (\pm 200 \text{ nm}, -8.5 \ \mu\text{m})$;
- PNJ scanning in 25 nm increments along the line L, parallel with the x-axis and 1 μm away from the micro-element

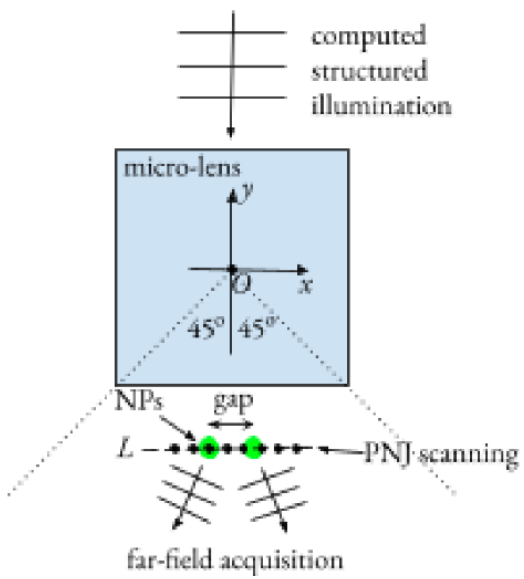

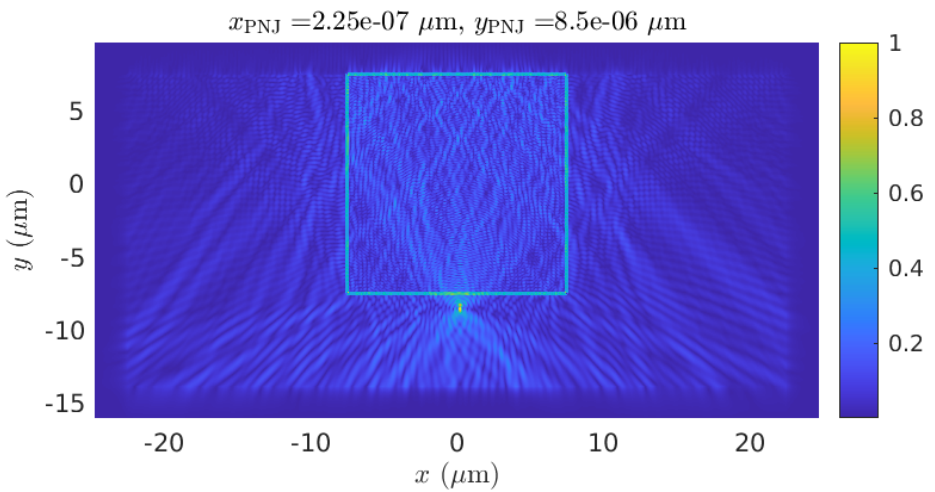

Resolving sub-classical lateral gaps

Karamehmedović and Hansen, Bremen Zoom Workshop 2023.

- for each PNJ illumination, $|E_{\text{far,NP}}|(\theta)$ and $|E_{\text{far,0}}|(\theta)$ are collected over the angle range $\pm 45^\circ$ from the negative y-axis, in 1° increments
- indicator function:

$$d = \frac{\| |E_{\text{far,NP}}| - |E_{\text{far,0}}| \|_2}{\|E_{\text{far,0}}\|_2} \approx \sqrt{\frac{\sum_{i=1}^{91} (|E_{\text{far,NP}}|(\theta_i) - |E_{\text{far,0}}|(\theta_i))^2}{\sum_{i=1}^{91} |E_{\text{far,0}}|(\theta_i)^2}}$$

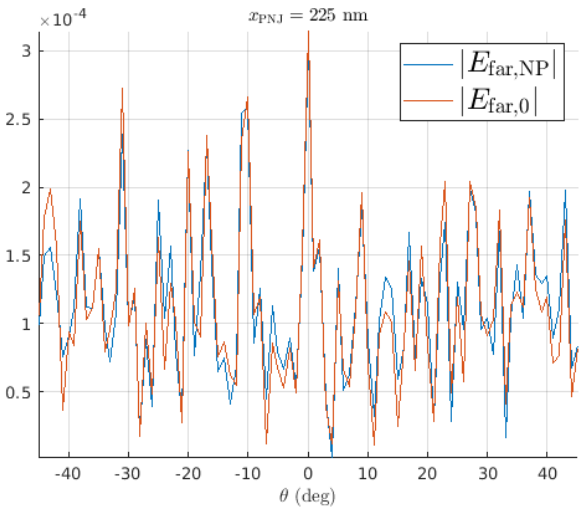

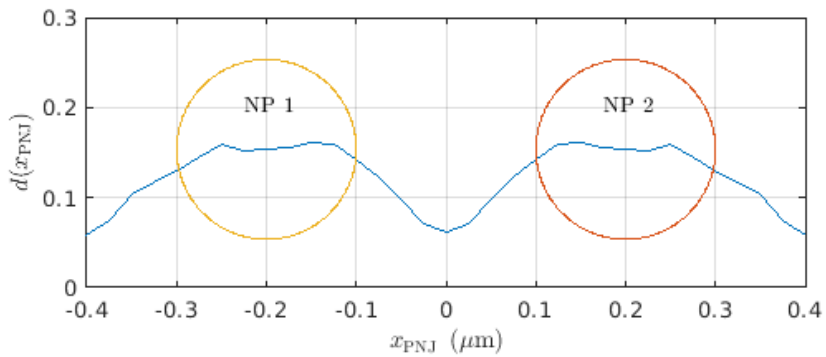

Conclusion

- achieved PNJ steering using (phase-only) computed illumination of a fixed homogeneous micro-element
- consistently narrow PNJ, large range of achievable PNJ positions
- the computed illumination can be realized using, e.g., one or two SLMs
- rapid scanning with a highly localized optical probe with no mechanical adjustment or translation of optical components or of the sample
- preliminary numerical results on super-resolution detection/measurement/imaging using PNJ scanning and far-field measurements (vertical as well as lateral)
- uncertainty quantification of practically achievable structured illumination of the micro-element
- larger micro-element may give a narrower PNJ and better resolution
- better indicator functions d
- imaging technique extendible to the 3D case